Available online at www.sciencedirect.com
ScienceDirect
International Journal of Heat and Fluid Flow 28 (2007) 178–190
International Journal of HEAT AND FLUID FLOW
www.elsevier.com/locate/ijhff

Convective heat transfer characteristics from combined mechanical and supply pulsed radial reattaching jets

J.S. Furlow [a], D.L. James [b,*]

[a] 846 TS USAF, 1521 Test Track Road, Holloman AFB, NM 88330, USA
[b] Texas Tech University, Box 41021, Lubbock, TX 79409-1021, USA

Received 19 August 2005; received in revised form 8 February 2006; accepted 8 February 2006
Available online 12 May 2006

Abstract

The heat transfer characteristics of combined mechanically and supply pulsated radial reattaching jets, CPRJR, were documented as a function of nozzle exit angle (0° and 20°), non-dimensional gap height (0.05 and 0.13), non-dimensional flow guide height (0.8 and 1.16), mechanical pulsation rate (5 and 10 Hz), mechanical to supply pulsation rate (1:1, 1:2, 1:3, and 1:4), phase angle (0° and 180°), and Reynolds number (1683 and 2366). Air was forced through a supply pulsation mechanism and then through a pulsated nozzle diverter apparatus. The air impinged on a heated plate where instantaneous heat flux and surface temperature measurements were collected and analyzed on instantaneous, ensemble-averaged, and area-averaged bases.

CPRJR heat transfer can be characterized as a frequency interference of mechanical and supply pulsation effects. Significant improvement, up to 72%, over the corresponding mechanical pulsation case was found to occur for a supply-to-mechanical ratio of 3:1 with a phase angle of 0°. In general, the increased heat transfer rates were associated with the an increase in surface-directed momentum caused by increased cycle "on" mass flow rate and corresponding entrainment.

Keywords: Convection heat transfer; Radial jet reattachment; Supply and mechanically pulsed; Jet impingement

1. Introduction

Convection heat transfer in modern industrial processes is used extensively in drying, cooling, and heating. Several types of jets have been used of which the various forms of inline jets have been most prevalent. For example, in a circular inline jet, a fluid exits a supply tube and impinges upon the given media forming a two-dimensional radial boundary layer that radiates from the centerline of the jet. The highest heat transfer and pressure force occur at or near the jet centerline. The surface pressure force exerted on the impinged media constitutes the fluid/media interaction. After the peak values, the Nusselt number and surface pressure both decrease outwardly in the radial direction.

For applications where large surface pressures are unwanted, e.g. drying or cooling of fragile surfaces, radial jets can be used. Radially reattaching jets are similar to inline impinging jets with the addition of a flow diverter at the end of the supply tube. The diverter causes the flow to turn and radially exit the jet at an exit angle, θ, relative to the horizontal. A sub-atmospheric pressure region is created directly under the diverter and causes the flow leaving the jet to turn downward with respect to its exit angle, that for appropriate conditions causes the jet to reattach on the impingement surface. The location where the flow reattaches at the impingement surface, R_r, creates the highest local pressure, and at or close to that location the greatest surface heat transfer. A theoretical analysis of laminar and turbulent radial jets by Page et al. (1989) indicated the degree to which the radial jet would curve towards the plate. This analysis evaluated the dependence of RJR flow field parameters on nozzle parameters including exit angle,

* Corresponding author. Tel.: +1 806 742 3563; fax: +1 806 742 3540.
E-mail addresses: scott.furlow@46tg.af.mil (J.S. Furlow), darryl.james@ttu.edu (D.L. James).

0142-727X/$ - see front matter © 2006 Elsevier Inc. All rights reserved.
doi:10.1016/j.ijheatfluidflow.2006.02.027

Nomenclature

A	area
b	nozzle gap
CPRJR	supply and mechanical pulsed radial jet
f	frequency of pulsation
FFT	fast Fourier transform
H	height, impingement surface to bottom of flow guide
k	thermal conductivity
Nu	Nusselt
PRJR	mechanical pulsed radial jet
PSD	power spectral distribution
r	radial coordinate
Re	Reynolds number $\frac{\rho \bar{V} b}{\mu}$
R_b	nozzle radius
R_c	radius of curvature of jet
R_r	reattachment radius
RJR	radial jet reattachment
SPRJR	supply pulsed radial jet reattachment
St	Strouhal number, $\frac{f_s \Delta b}{V}$
$\bar{V}$	average jet exit velocity
Δ	change in
θ	nozzle exit angle relative to horizontal, + towards plate
ξ	generalized radial position on impingement plate
$\phi(t)$	time-varying crank angle position
ω	phase angle

Subscripts

mch	mechanical
s	supply
min	minimum gap spacing

nozzle radius and height per exit gap, gap Reynolds number, and a turbulent spread parameter. The reattachment of the flow creates a region of low-pressure recirculation that is dominated by a toroidal vortex, Agnew et al. (1992), and was shown experimentally by Castleberry (1997) to be a stagnant area of low local Nusselt numbers in comparison to all other local Nusselt numbers over the impingement surface.

A general radial jet schematic depicted in Fig. 1 shows the reattachment radius, R_r, radial coordinate, r, the nozzle radius, R_b, gap height, b, the flow guide height, H, and the radius of curvature of flow, R_c. Also shown is the low pressure region that constitutes the stagnation region bounded by R_r on all sides. For some conditions, radial reattaching jets provide equal to or higher radial Nusselt values in comparison to inline impinging jets for the same Reynolds number and non-dimensional flow guide height, H/R_b, conditions as shown experimentally via a literature review by Page (1993), experimentally by Seyed-Yagoobi et al. (1998), and numerically by Laschefski et al. (1992).

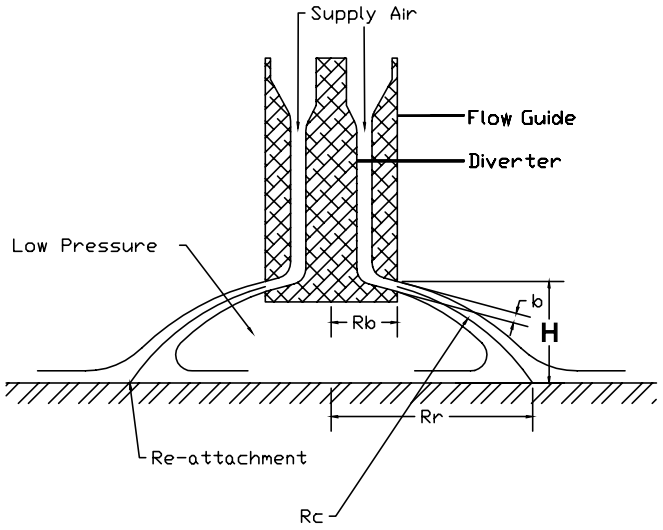

Fig. 1. General radial jet reattachment flow schematic (3).

Ostowari et al. (1987) showed that the flow guide height has a significant effect on R_r and Nusselt numbers. Laschefski et al. (1995) showed that radial exit angles between −10° and 60° produced Nusselt values between 50% and 115% of the inline impinging Nusselt value with a lower average pressure for the respective ranges in laminar submerged jet flows. Seyed-Yagoobi et al. (1998) compared heat transfer characteristics from radial jet and inline jet nozzles. They found enhancement in convective heat transfer occurred with a +45° exit angle for a height to diameter ratio of 0.5; no enhancement occurred for the 0° or −10° exit angle.

The heat transfer rates of inline free jets were shown to be improved by intermittent flow pulsation frequencies in excess of a critical Strouhal number by Zumbrunnen and Aziz (1993). Conversely, in instances of sub-critical pulse rates, the pulsation of impinging inline free jets can lead to reduced convective heat transfer. For sinusoidally pulsed inline free jets, the heat transfer rates have been shown to be reduced by as much as 17% while square wave pulsations have been shown to increase the stagnation heat transfer coefficients by as much as 33% for Strouhal numbers greater than 0.26, Sheriff and Zumbrunnen (1994). It has been shown by Nevins and Ball (1961) that for pulsed submerged inline jets, the Nusselt number was independent of pulsation frequency (between 0 and 18 Hz) for sinusoidal, square, and triangular pulsed profiles.

Improvements in RJR heat transfer within the stagnation region by means of mechanical pulsation of the diverter, that is the moving of the diverter up and down and

referred to as PRJR nozzles, were sought experimentally by Castleberry (1997) and James et al. (1999). Pak et al. (1999) simulated flow exiting PRJR nozzles to better understand the flow field in the region beneath the nozzles. Their work showed that local time averaged Nusselt numbers for PRJR (mechanically pulsed radial jet reattachment) nozzles were enhanced in the swept region of the recirculation region, but these gains were usually offset by Nusselt number decreases in other regions of the flow field. The mechanical pulsing of the nozzle swept the reattachment radius towards and away from the nozzle centerline as a function of time and was directly related to nozzle pulsation as shown by Furlow and James (1999). The time-averaged Nusselt numbers were typically bounded by the non-pulsed cases at the higher limit by the corresponding minimum gap case and at the lower limit by the corresponding maximum gap case.

Agnew et al. (1992) used supply pulsations to radial jet nozzles to attempt to increase heat transfer under RJR nozzles. They reported a limiting frequency, dependent on velocity and nozzle height, above which no reattachment radius forms. From Agnew's study, the turbulence intensity near the surface was shown to be enhanced due to a highly irregular flow. The authors reasoned that the increased turbulence induced higher heat transfer; however, Bremhorst and Agnew (1999) showed that for the supply pulsation frequencies between 5 and 40 Hz, no enhancement was realized. The supply pulsation resulted in averaged convective heat transfer results equal or less than the respective steady RJR nozzle as the supply pulsation effects did not disrupt the forming of a boundary layer downstream of the impingement radius.

Continuing efforts to improve heat transfer under RJR nozzles is the thrust of this work. Because mechanical pulsation did improve local instantaneous heat transfer within the pulsation cycle, it is proposed that the combination of supply and mechanical pulsation could induce instability in the flow that leads to greater instances of the stagnation area being refreshed via blowout. Also combined pulsation could provide a mechanism for increasing the heat transfer in the portions of the mechanical pulsation cycle where the Nusselt value is reduced. This paper presents the results of a study of a supply and mechanical combined pulsed radial jet reattaching, referred to as CPRJR, nozzle to determine the effect on impingement surface heat transfer as a function of pulsation amplitude, frequency, phase angle, Reynolds number and nozzle geometry. The convective heat transfer is evaluated from the surface and air temperature and surface heat flux measurements.

2. Experimental apparatus and procedure

A schematic overview of the overall CPRJR test setup is shown in Fig. 2. The CPRJR nozzle system used many of the same elements as described in the PRJR system of James et al. (1999) with the addition of a supply pulsation mechanism. The CPRJR nozzle consisted of a 40.4 mm diameter tube, approximately 15 diameters long, that contained replaceable diverters and flow guides. The diverters were made with various exit angles of which the 0° and 20° exit angle were used in this work.

Mechanical pulsations of the diverter were achieved using an offset link and chain mechanism. The mechanical pulsation rate was monitored and adjusted based on the frequency output of a photo-interrupt sensor and were within 0.1 Hz of their target frequency. The minimum and maximum gap heights correspond to nozzle crank angles of 0° and 180°, respectively. Supply pulsations were achieved by rotating different slotted disks through a small gap in the air line, see Fig. 2. The rotating disks were mounted on the same shaft as the mechanical pulsation shaft that provided a supply pulsation frequency equal to the mechanical pulsation frequency with an accurate phase adjustment between the two. Each rotating disk had uniform angular slots cut in the radial direction. The slots were cut such that the areas through which flow was allowed were equal in area to the sections of the disk that blocked flow. This produced equal on-to-off ratios.

Four separate disks were manufactured that provided supply pulsed flow of 1, 2, 3, and 4 times the mechanical pulsation rate. The disks were moveable with respect to angular position on the supply pulsation shaft to provide a phase shift with respect to mechanical pulsation (e.g. flow through the nozzle could be specified with respect to the location of the diverter). For any supply-to-mechanical pulsation ratio, the mechanical pulsation frequency served as the basis frequency in the ensemble-averaging algorithm as it was the lowest input frequency possible for any supply-to-mechanical pulsation ratio.

Air was supplied to the CPRJR nozzle using a compressor. The air flowed through a pressure regulator, an air dryer, a settling tank, and then traveled to the experimental equipment where the mass flowrate was controlled by a pressure regulator and ball valve. The air entered the supply pulsation mechanism, then the rotameter (used to set the flow rate when the flow was not pulsed) and finally into the annular supply tube that contained the flow guides and diverter. Due to the many internal cross sectional changes and complex internal geometry, the flow was turbulent at the exit of the diverter for the steady RJR flow and for the steadily pulsed CPRJR and PRJR flows. Turbulent intensity (TI) values were obtained using a single hot-wire probe located at mid-height of the nozzle exit within 1 gap width. TI values for the pulsed flows (CPRJR and PRJR) were obtained by forming the standard deviation between a moving average of twenty data points and the instantaneous velocity $V(t)$ divided by the moving average. The moving average at time t, $\overline{V(t)}$, was calculated by averaging the 10 data points immediately prior to and after a particular point in time (sampling rate was 20 kHz); thus $\mathrm{TI} = \sqrt{(V(t) - \overline{V(t)})^2}/\overline{V(t)}$. The resulting TI values varied between 21% and 32%. CPRJR flows had slightly larger TI

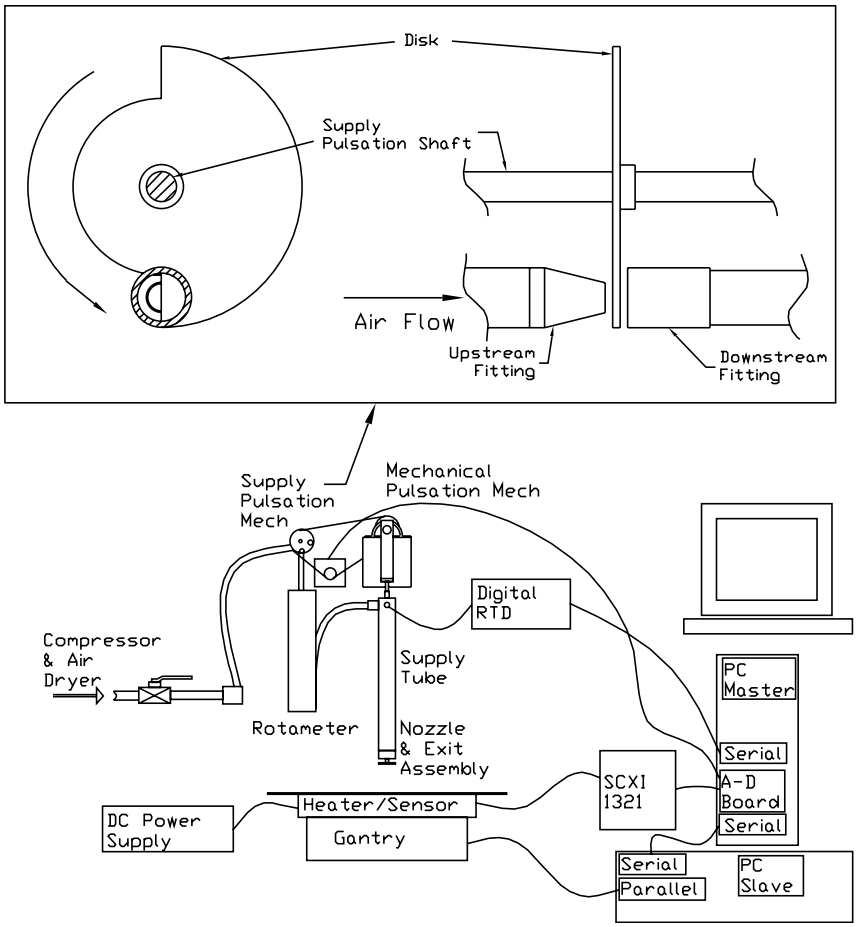

Fig. 2. Experimental setup and schematic of supply pulsation mechanism.

values than the purely mechanical pulsation found in PRJR flows.

A heater plate was designed to house a Vatell surface heat flux microsensor and to serve as the heated impinging surface for the reattaching jets. The heater plate was machined from medium carbon steel and measured 266.7 mm wide by 406.4 mm long by 36.83 mm thick. The plate was cut into two pieces with the larger piece of width 209.5 mm and the smaller piece of width 57.2 mm. The off-center lengthwise cut was made to provide a means of sandwiching the microsensor between the two pieces in an accurate manner so that any gaps between the sensor and the plate were minimized. The precise mating of the two plates and the sensor ensured that the surface was smooth so that no boundary layer interruption due to sensor misalignment or varying plate roughness occurred. Thermal paste was used to fill any air gaps between the two plates, heater, and sensor. An electric heater unit with a maximum power density of 15.5 kW/m^2 was given a light coat of thermal paste and was fitted to the bottom of the heater plate. Insulation was placed on all but the top surface such that only the top surface of the heater plate lost energy. A computer controlled gantry moved the heater plate assembly in the x- and y-directions underneath the nozzle.

Instantaneous heat flux and surface temperature data were acquired using the heat flux microsensor and analog to digital conversion equipment. The microsensor was 6.35 mm diameter had a surface area of 31.7 mm^2 and was covered with a Zynolyte coating of emissivity of 0.94. The microsensor had a time constant of 6 ± 2 μs. A digital RTD was placed directly upstream of the supply tube to measure the supply air temperature. Exit velocity was recorded using a TSI Incorporated IFA-100 flow analyzer and a 1210-20 model single hot film probe. The diverter was carefully aligned with the flow guide to ensure that the axis-symmetric conditions reported for reattaching radial flow by Castleberry (1997) and Ostowari et al. (1987) was achieved. Axis-symmetry was utilized as data were obtained in a straight line outward from the nozzle centerline to several nozzle diameters.

2.1. CPRJR flow characterization

Hot film measurements using a single-film probe placed 5 mm from the nozzle exit were used to obtain the magnitude of the exit velocity and the corresponding turbulence intensity for pure supply pulsation. The single-film probe was oriented horizontally. The diverter and flow guide were set to an exit angle of 0°. The nozzle gap measured 5.88 mm

corresponding to an average of the corresponding mechanical case of non-dimensional gap height, b_{min}/R_b, of 0.13. The non-dimensional flow guide height, H/R_b, was set to 1.16. The flow was maintained at a nozzle gap based Reynolds number of 2366. The *Re* was calculated from the average steady non-pulsed exit velocity of the system. This calculation allowed the *Re* to be based on the average nozzle exit velocity from the pulsed system over one pulsation cycle. The air supply was pulsed continuously at frequencies, f_s, of 10, 20, 30, and 40 Hz. The jet exit velocity measurements were made at a constant data acquisition rate of 4000 Hz.

CPRJR nozzle flow combines both supply and mechanical pulsation. To investigate the exit velocity and turbulence intensity for combined pulsation, the test conditions used in supply pulsation were maintained with the addition of mechanical pulsation, f_{mch}, at 10 Hz. The flowrate measurement method for the combined pulsation case was to set the nozzle gap to the median position and the supply pulsation plate to an "on" position. The mass flow rate was adjusted to maintain the same cycle averaged value used for pure mechanical pulsation (i.e. PRJR flow). The phase angle was defined as the crank angle position relative to flow "on". The phenomenon of phase angle variance was investigated as the phase angle, ω, was set to either 0° or 180° for any supply-to-mechanical pulsation ratio. At a supply-to-mechanical ratio of 1:1 the variation in ω caused the flow to turn "on" in the mechanical pulsation region of maximum to average gap height, $\omega = 0°$, or at the region of average to minimum gap height, $\omega = 180°$, illustrated in Fig. 3(a). Fig. 3(a) displays the diverter position in relation to the angular slots in the 1:1 supply-to-mechanical ratio. In region 1, denoted by the corresponding circled number, of Fig. 3(a) the flow is off for the $\omega = 0°$, and on for the $\omega = 180°$ case. As the diverter moves down the flow-off slot blocks the flow and then the flow is allowed to pass as the "on slot" is moved into the pipe's separation. Once the diverter reaches maximum gap, b_{max}, the diverter moves up and the process is reversed.

The supply-to-mechanical pulsation ratio of 2:1 produced pulsation patterns different from the 1:1 ratio. Fig. 3(b) shows the diverter position in relation to the supply pulsation pulsed flow. Region 1 for $\omega = 0°$ represents the "on slot" of the supply pulsation mechanism. The 2:1 supply-to-mechanical ratio is similar to the 1:1 supply-to-mechanical ratio case except that the geometry of the supply pulsation disk allows flow or no flow at both the maximum and minimum gap depending on phase angle.

The supply-to-mechanical ratio case of 3:1 is very similar to the 1:1 ratio case. The relation of diverter position to supply pulsation appears in Fig. 3(c). The most notable difference between the 3:1 ratio and 1:1 ratio case is the increase in the number of times that the flow is switched on and off. In Fig. 3(c), regions 2 and 3 represent extra on-off "switches" when compared to the 1:1 ratio case of Fig. 3(a).

The supply-to-mechanical ratio case of 4:1 is very similar in function to the 2:1 ratio case. The relation of diverter position to supply pulsation appears in Fig. 3(d). The additional pulsing of the flow that is represented by the extra

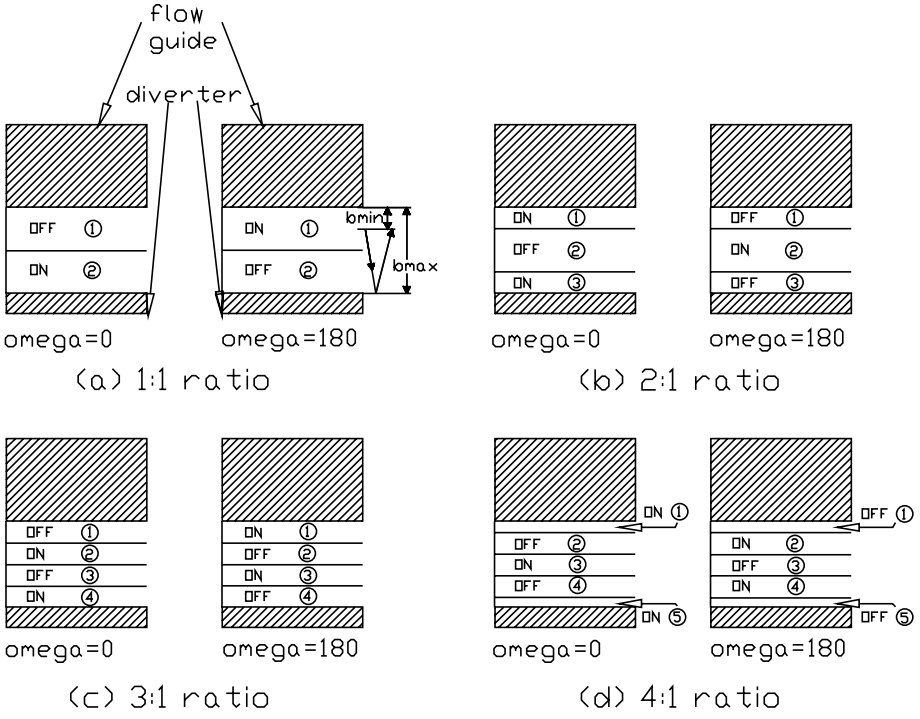

Fig. 3. Diverter position showing flow "on" and "off" conditions for the various supply to mechanical pulsation ratios.

"switches" of regions 4 and 5 and the altered duration of region 1 when compared to the 2:1 ratio case comprise the differences between the two ratios.

2.2. Data reduction

Convective heat transfer was calculated using the heat flux microsensor and the data acquisition system to acquire instantaneous heat flux and surface temperature data as a function of radial position, r, and time dependent nozzle crank angle position, $\phi(t)$. The heater plate was well-insulated on all but the top surface, thus the heat input by the heater pad was convected and radiated to the environment at the top surface. The convective heat flux was calculated by subtracting the radiation heat flux from the surface heat flux data. Heat flux and surface temperature data were acquired at a rate of 20 kHz. Ensemble-averaging of the heat flux and temperature data was used to calculate a local convective heat transfer coefficient, $h(r,\phi(t))$, as a function of the time dependent crank angle (diverter) position by averaging the instantaneous heat flux and surface temperature data using points equi-distant with respect to time within a discretized series of steady periodic data at the primary frequency present over 300 cycles. Because the mechanical forcing frequency was always the primary frequency, it was used as the fundamental frequency from which the data was reduced. Thus the local convective heat transfer coefficient is

$$h(r,\phi(t)) = \frac{q''_{\text{sensor}}(r,\phi(t)) - q''_{\text{rad}}}{T_s(r,\phi(t)) - T_\infty} \tag{1}$$

The local Nusselt number is formed using the nozzle radius

$$Nu(r,\phi(t)) = \frac{h(r,\phi(t))R_b}{K_{\text{air}}} \tag{2}$$

A local, cycle-averaged convective heat transfer coefficient was calculated by integrating the local, quasi-steady data over one period

$$\bar{h}(r) = \frac{1}{2\pi}\int_0^{2\pi} h(r,\phi(t))\mathrm{d}\phi \tag{3}$$

Finally, the average convective heat transfer coefficient can be calculated from the local, cycle-averaged value by first defining an average surface temperature

$$\overline{(T_s - T_\infty)} = \frac{2\pi}{\pi R^2}\int_0^R (T_s(r) - T_\infty) r\mathrm{d}r \tag{4}$$

and with the average convective heat transfer coefficient defined as

$$\bar{h}A\overline{(T_s - T_\infty)} = \int_0^R \bar{h}(r)(T_s(r) - T_\infty)2\pi r\mathrm{d}r \tag{5}$$

substituting Eq. (4) into Eq. (5) yields

$$\bar{h} = \frac{\int_0^R \bar{h}(r)(T_s(r) - T_\infty) r\mathrm{d}r}{\int_0^R (T_s(r) - T_\infty) r\mathrm{d}r} \tag{6}$$

In previously published papers on RJR heat transfer (5) and (7), the average convective heat transfer coefficient was defined using the following equation:

$$\bar{h} = \frac{1}{A}\int_0^{\xi} \bar{h}(r)2\pi r\mathrm{d}r \tag{7}$$

Eq. (7) is used in this work in order to compare heat transfer coefficients from the previously published work. The difference in average convective heat transfer coefficient calculated using Eqs. (6) and (7) varied between 0% and 7%, with an average difference of less than 2%.

2.3. Uncertainty

An uncertainty analysis was performed following the general error propogation given by Beckwith et al. (1993). All uncertainty calculations were evaluated at a confidence level of 95%. After oversampling and ensemble-averaging, instantaneous uncertainties for the surface temperature, surface heat flux, and heat transfer coefficient were ±0.4%, 2.1%, and 2.2% respectively. Several tests were performed and the mean uncertainty in the average convective heat transfer coefficient and Nusselt number were ±4.5% and ±6.9%, respectively. Uncertainty in the nozzle to plate orthogonality was ±1% and in the gantry position was ±0.13 mm.

3. Results and discussion

The purpose of combined pulsation mechanisms was to evaluate and characterize the surface heat transfer from a CPRJR nozzle. To report the heat transfer characteristics from CPRJR nozzles, instantaneous surface temperature and heat flux measurements were made at the impingement surface. The exit velocity magnitude and turbulence intensity was measured in order to characterize the flow leaving the CPRJR nozzles and to determine pulsation interaction and frequency dependence.

3.1. Heat flux quantification

Heat flux quantification measurements were made to verify the accuracy of the heat flux and surface temperature sensor values. Two steady flow RJR cases were evaluated with the following parameters: a Re of 2366, an exit angle of 0°, a non-dimensional gap height, b/R_b, of 1.161, and non-dimensional flow guide heights, H/R_b, of 0.131 and 0.439. To correlate the total input electrical power to the measured heat flux over the impingement area, the total input electrical power was measured resulting in a heat flux of 3500 W/m^2. The total electrical power input was calculated and compared to the experimentally measured convective heat transfer rate that was obtained by integrating the experimentally calculated convective heat flux over the impingement area as reported in Furlow (1999). The deviation in power input compared to convective heat

transfer rate out of the plate was −2.25% and +0.7%, for the two cases tested, and falls within the uncertainty for heat flux.

3.2. Hot film measurements

To quantify the effects of varying the phase angle, ω, and the supply frequency, hot film velocity measurements were made of supply and combined pulsation at a point one gap height from the nozzle exit at a sampling rate of 4 kHz.

3.2.1. Supply pulsation

Nozzle exit velocity measurements were made for supply pulsation frequencies of 10 Hz, 20 Hz, 30 Hz, and 40 Hz. The diverter exit angle was set to 0°, the non-dimensional flow guide height was set to 1.161 and the non-dimensional gap height was set to 0.285, corresponding to the mean gap height of the PRJR (mechanical pulsation) case and the nozzle gap. The nozzle exit velocity magnitude are shown for a 1 s interval in Fig. 4 for a 10 Hz pure supply pulsation.

Fig. 4 shows an initial spike in nozzle exit velocity that corresponds to the sudden release of pressure as the disk opens and releases pressure built up behind the flow-off disk section. The basic periodic nozzle exit velocity shape seen in Fig. 4 is indicative of the basic repeated nozzle exit velocity shapes seen in higher frequency supply pulsations of 20 Hz, 30 Hz, and 40 Hz. The trend established in the four pure supply pulsation cases induces a nozzle exit velocity shape that is between a sawtooth and a square wave excepting the initial spike at the onset of flow-on. Clearly seen in Fig. 4 is a small velocity spike that occurs in the flow-off region. This spike is due to the interaction of the vortices above and below the nozzle exit gap. As the supply pulsation mechanism suddenly stops the flow, air is entrained and pulled across the hot film replacing the vanishing jet.

A frequency analysis of the nozzle exit velocity data produced power spectrum distribution, PSD, for the four supply pulsation frequencies. Present in all PSDs were noticeable returns at integer multiples of the supply pulsation frequency that are indicative of the Fourier representation of the input due to the manner in which the supply was pulsed. Referring to Fig. 2, the flow was forced "on" and "off" by the rotating disk producing odd and even harmonic overtones, because of the nearly symmetric flow that is generated per disk revolution, except for the initial on and off portions of the flow.

3.2.2. Combined pulsation

Combined pulsation nozzle exit velocity measurements were made using the same nozzle and geometric parameters as the supply pulsation experiment excepting the addition of mechanical pulsation at 10 Hz. The phase of the supply pulsation with respect to mechanical pulsation was set to

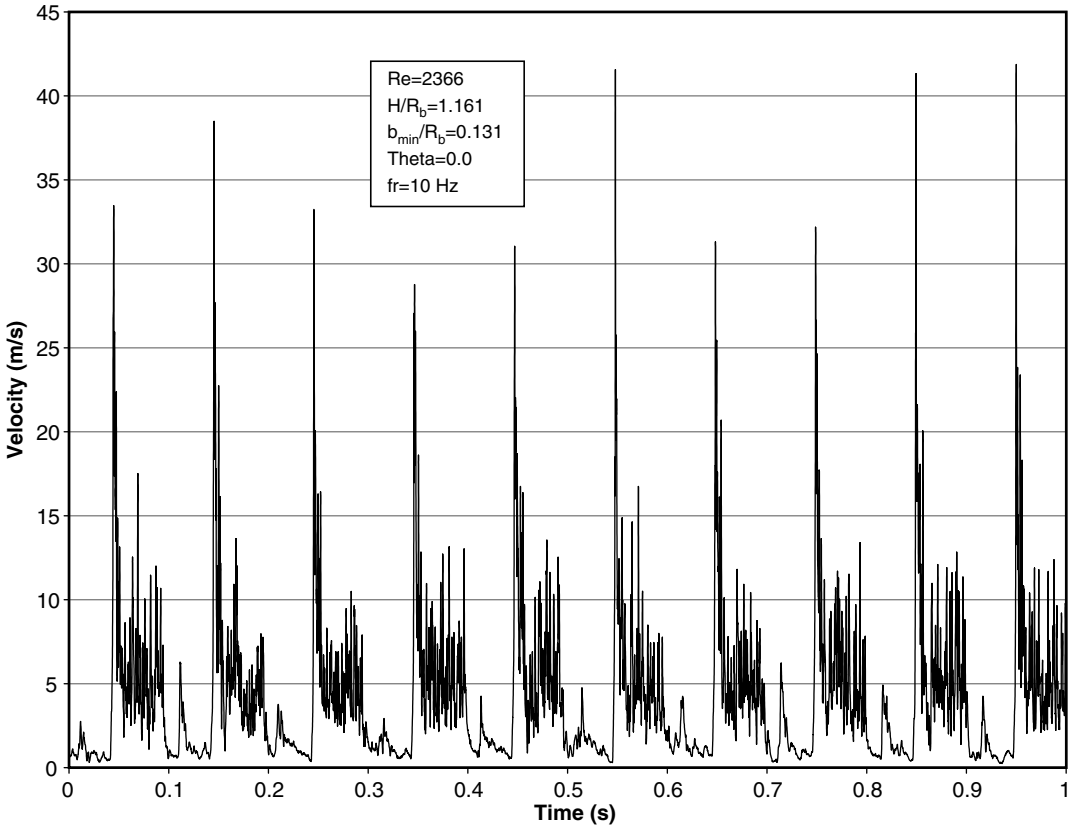

Fig. 4. Nozzle exit velocity magnitude for the 10 Hz pure supply pulsation case.

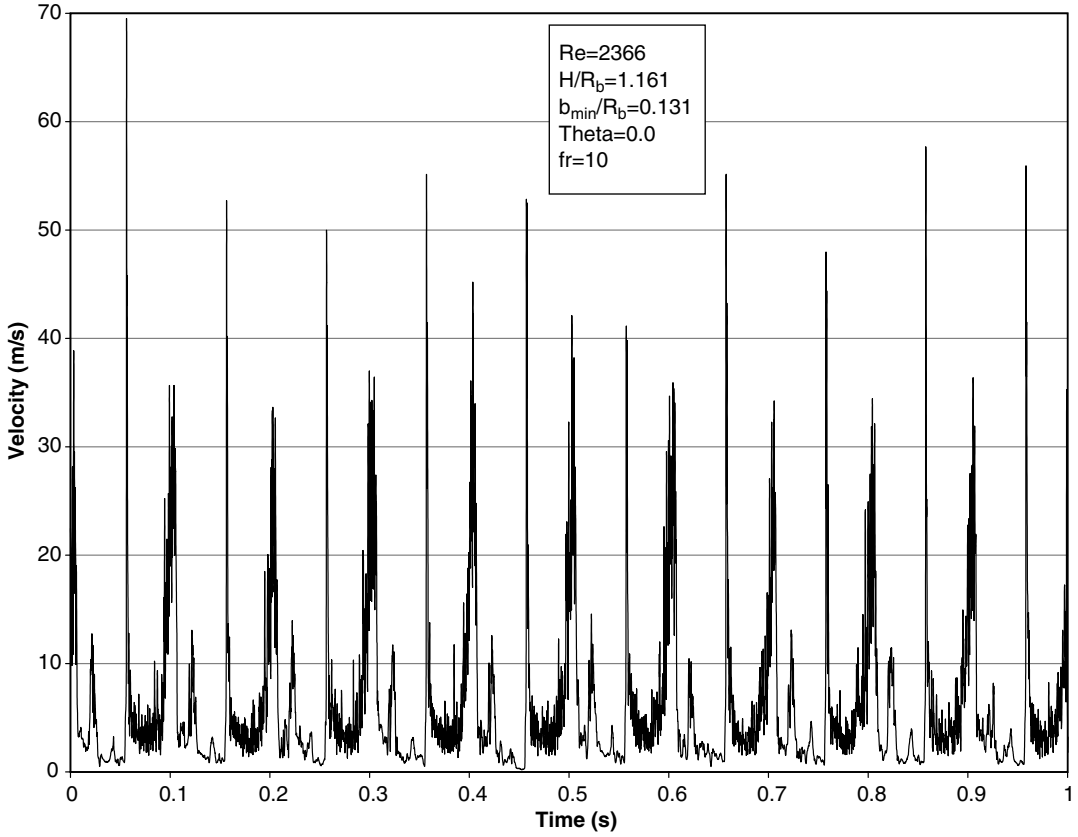

Fig. 5. Nozzle exit velocity magnitude for the 1:1 ratio, $\omega = 0°$ CPRJR flow.

either 0° or 180°. The phase angle value of 0° corresponded to the center of the flow-on slot in the rotating disk (see Fig. 3) occurring at the same time in the pulsation cycle as the maximum gap. The phase angle value of 180° corresponded to the center of the flow-on slot occurring at the minimum gap position in the mechanical pulsation cycle. Each supply-to-mechanical-pulsation ratio was evaluated at phase angles of 0° and 180°.

For the supply-to-mechanical ratio 1:1 $\omega = 0°$ case, Fig. 5 shows a general increase in the magnitude of the peak nozzle exit velocity when compared to the nozzle exit velocity of the corresponding supply pulsation case seen in Fig. 4. However, the velocity in the flow-on region between the two peaks is very low. The low magnitude of velocity indicates a frequency and phase angle effect that decreases the exit velocity. Conversely in the nozzle exit velocity of the $\omega = 180°$ case, there is an enhancement in the average nozzle exit velocity during the flow-on portion of about 100% when compared to the $\omega = 0°$ case. This was due to the fact that the exit area was smaller during flow-on for the $\omega = 180°$ case. The flow-on region retains some of the saw tooth shape seen in the corresponding supply pulsation case of Fig. 4. The trends established by the supply-to-mechanical ratio of 1:1 are indicative of the 3:1 ratio nozzle exit velocity.

The 2:1 supply-to-mechanical ratio nozzle exit velocity profile shows a similar increase in the values of peak nozzle exit velocity magnitude by about 100% for the $\omega = 0°$ case and 75% for the $\omega = 180°$ case when compared to the corresponding supply pulsation case. The higher peak nozzle exit velocity associated with the phase angle, $\omega = 180°$, in the 1:1 ratio appears at the phase angle of 0° in the 2:1 ratio as this phase corresponds to an open minimum gap. Again the result of increased peak nozzle exit velocity magnitude was due to pressure release at the smaller gap height within the mechanical pulsation cycle. The trend prevalent with the 2:1 ratio is indicative of the behavior of the 4:1 ratio except that the nozzle exit velocity distribution occurs twice as fast.

PSD analyses of the nozzle exit velocity for the 1:1 case show that the 10 Hz phenomenon is dominant. The PSD analyses for the 2:1 ratio case indicate a strong supply frequency dominance, 20 Hz, of the nozzle exit velocity. PSD data for the 3:1 ratio case $\omega = 0°$, demonstrate a trend where mechanical pulsation, 10 Hz, is dominant with significant 30 Hz contribution. In the PSD data for the 3:1 ratio $\omega = 180°$, and both phase angles in the 4:1 ratio cases, the maximum PSD occurs at the supply frequency, 30 Hz or 40 Hz, with some significant 10 Hz contribution.

PSD results indicated that the flow at the nozzle exit is driven by one or both pulsation mechanisms with possible overtones caused by the non-linearity of the flow. These results also indicate that input pulsation frequency phenomena are present at the nozzle exit. The influence of the mechanical forcing frequency was present in all PSD

data and was indicative of the motion of the diverter and of the FFT analysis of strongly periodic fluid flow.

3.3. Nusselt number measurements

Time varying CPRJR nozzle flow interactions with the heated plate produced variations in heat transfer that were recorded via local instantaneous heat flux and surface temperature measurements. Local instantaneous heat transfer characteristics were ensemble-averaged over many cycles and reported as local Nusselt numbers. Experimental cases were run that identified the influence on heat transfer as a function of mechanical and supply pulsation, Reynolds number, non-dimensional flow guide height, non-dimensional gap height, and nozzle exit angle. The values of these parameters that were tested are: Re of 1683 and 2366, H/R_b of 0.81 and 1.161, b_{min}/R_b of 0.131 and 0.05, θ of 0° and 20°, f_{mch} of 5 Hz and 10 Hz, f_s/f_{mch} of 1:1, 2:1, 3:1, 4:1 (Strouhal numbers based on the gap displacement and average exit velocity, $St = f_s \Delta b/\bar{V}$, range from 0.01 to 0.04), ω of 0° and 180°. The non-dimensional flow guide height was coupled to the non-dimensional gap height and the two were not varied independently of each other. Experimental cases were run in which all combinations of supply pulsation frequency, f_s, phase angle, ω, nozzle exit angle, θ, and mechanical pulsation frequency, f_{mch} were varied for the Re number of 2366 and the lower values of non-dimensional flow guide and gap height. Cases were also run at the higher values of non-dimensional flow guide height, 1.16, and non-dimensional gap height, 0.13, Re of 2366, mechanical pulsation frequency of 10 Hz, and exit angle of 0° for all combinations of supply pulsation frequency, and phase angle. For the lower Re number value of 1683 all combinations of supply pulsation frequency, phase angle and exit angle were varied for cases where the mechanical pulsation frequency was 10 Hz, the non-dimensional flow guide height was 0.8, and the non-dimensional gap height was 0.05.

In comparing heat transfer from SPRJR (pure supply pulsed), CPRJR (combined mechanical and supply pulsed), and PRJR (pure mechanical pulsed) nozzles, all parameters can be directly compared except for flow rate. Flow rates in CPRJR and SPRJR nozzles are different from PRJR nozzles because the flow rate is time varying with respect to the nozzle gap. A gap height based Reynolds number can be reported for PRJR nozzles as the velocity is directly related to the flow rate and changing gap height through the nozzle gap exit area, Castleberry (1997). However an equivalent PRJR-based Reynolds number is not possible with supply and combined pulsation as the supply pulsation mechanism is not related to the nozzle gap height in a manner that allows the mechanical pulsation Reynolds number to be consistently applied. To give an accurate correlation between supply, combined, and mechanical pulsation, a cycle average flow rate was used. As the angular duration of the supply pulsation "on" and "off" segments were equal, the averaged flow rate during the "on" portion was twice the value of the mechanical equivalent. This technique yielded a combined pulsation cycle averaged Re equal to the corresponding mechanical pulsation Re. It should be noted that basing Re on the cycle averaged flow rate yields a value that is up to five to ten times smaller than a Re based on the maximum velocity in a cycle.

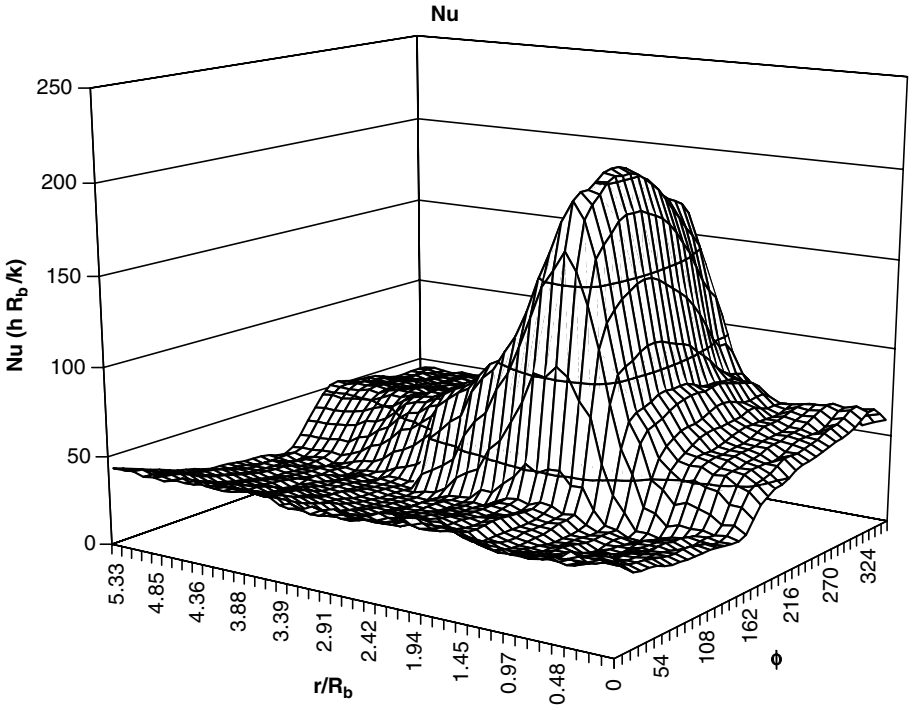

Fig. 6. CPRJR local Nu number profile for the 1:1 ratio, $\omega = 0°$ case.

3.3.1. CPRJR nozzle heat transfer characteristics

Heat transfer data are reported as *Nu* number surface plots for local heat transfer data and as 2-D plots for averaged heat transfer data. The formulation of *Nu* number involved the use of constant R_b and k in Eq. (2), therefore the convective heat transfer coefficient, h, is directly comparable to the *Nu* number.

CPRJR heat transfer is characterized by *Nu* number extremum with movement of the reattachment radius during flow-on conditions. Local instantaneous *Nu* plots are

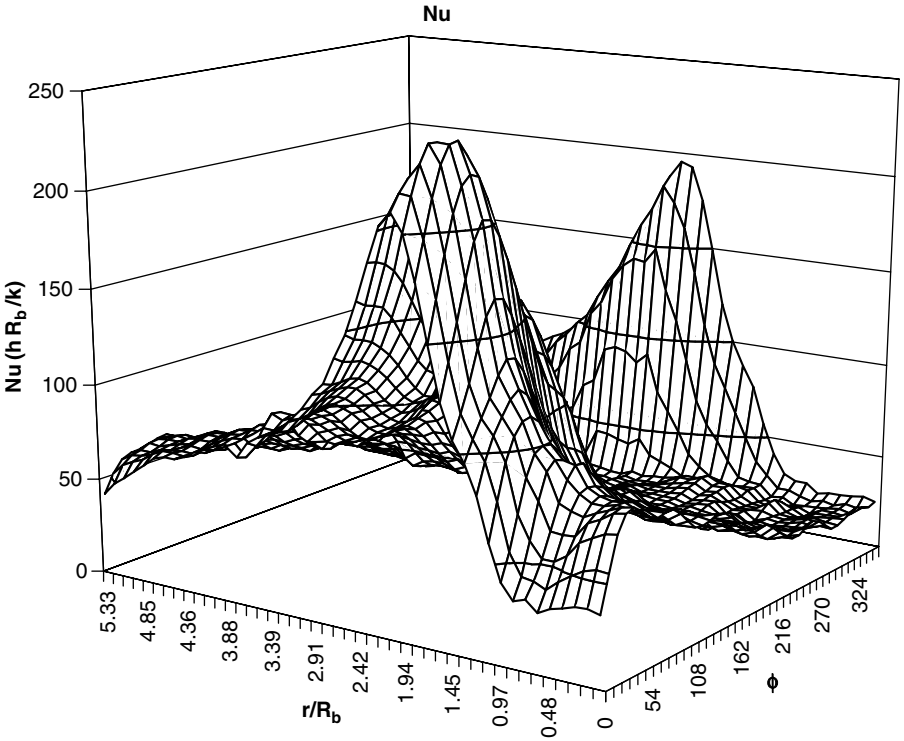

Fig. 7. CPRJR local *Nu* number profile for the 1:1 ratio, $\omega = 180°$ case.

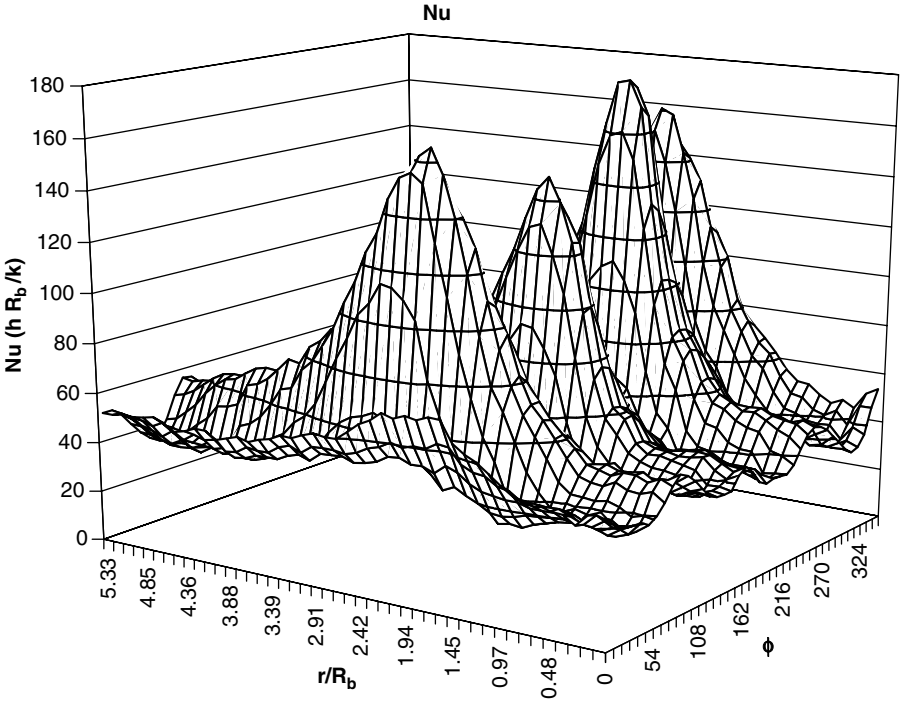

Fig. 8. CPRJR local *Nu* number profile for the 4:1 ratio, $\omega = 0°$ case.

presented in Figs. 6–8 for which $Re = 2366$ and $f_{mch} = 10$ Hz; additionally $H/R_b = 1.161$, $b_{min}/R_b = 0.131$, and θ of 20° in Fig. 6, and $H/R_b = 0.8$, $b_{min}/R_b = 0.05$, and $\theta = 0°$ in Fig. 8. The difference between Figs. 6 and 7 is the phase angle, ω, that is 0° or 180°, respectively. Present in combined pulsation *Nu* data is the distinct formation of a reattachment region as seen in Figs. 6–8 by the region of high *Nu* during flow-on portions of the cycle. The constant presence of a reattachment radius, defined in this work by the maximum in *Nu* values, during the flow-on portions indicates that the experimental conditions were such that the jet reattached on the impingement surface and velocity and thermal boundary layers formed distinct regions inside and outside of the reattachment radius.

Movement of the reattachment radius was caused by the mechanical pulsation effects of the diverter motion. The radial location of the maximum *Nu* value changed from a minimum value of about 10% in the 1:1 cases (e.g. Fig. 6) to a maximum value of about 30% (e.g. Fig. 8) in the 4:1 cases. Supply pulsation effect did not move the reattachment radius and only produced extreme values in heat transfer. The combined pulsation heat transfer can be

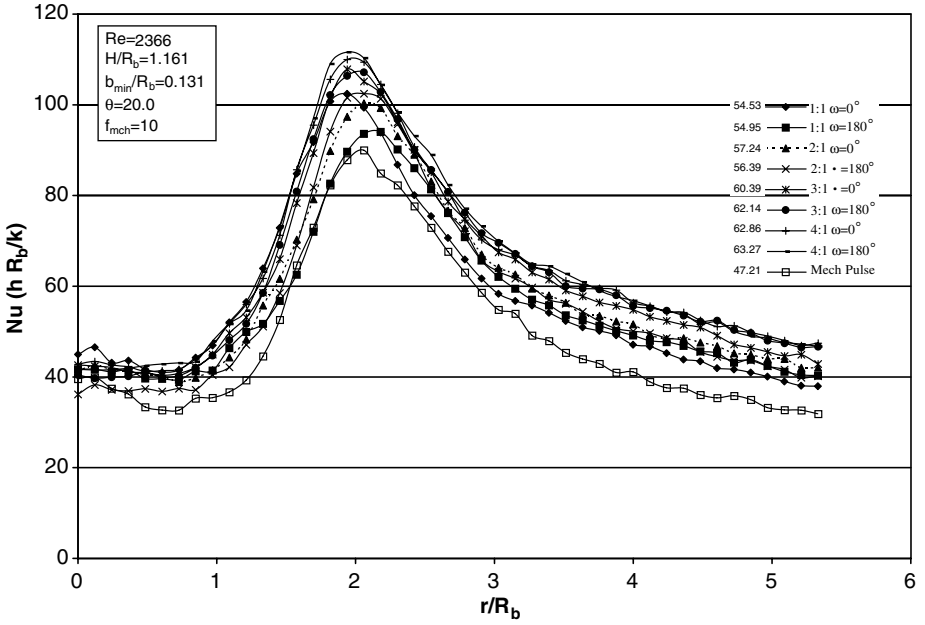

Fig. 9. CPRJR averaged *Nu* number for $Re = 2366$, $H/R_b = 1.161$, $b_{min}/R_b = 0.131$, $\theta = 20$, $f_m = 10$ Hz.

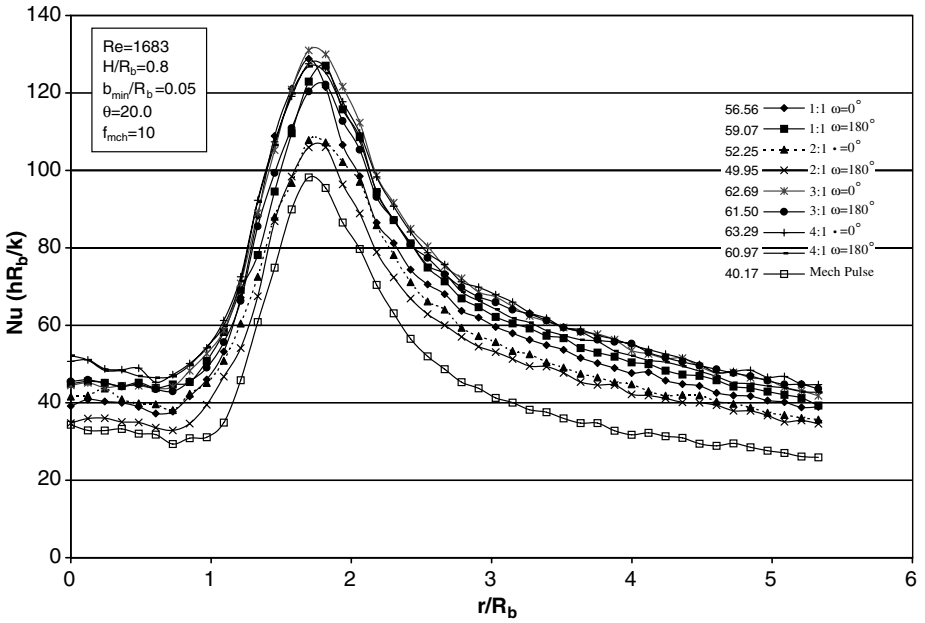

Fig. 10. CPRJR averaged *Nu* number for $Re = 1683$, $H/R_b = 0.05$, $b_{min}/R_b = 0.05$, $\theta = 20$, $f_m = 10$ Hz.

thought of as a frequency interference of the mechanical and supply pulsation effects.

The frequency dependence of *Nu* number was documented via a PSD analysis performed on heat flux at each radial coordinate. The supply pulsation component dominates the frequency of measured *Nu* number; thus the mechanical pulsation frequencies studied, f_{mch} of 5 Hz and 10 Hz, were found to have little direct effect on heat transfer. Typical influence of supply pulsation frequency, f_s, is shown in the instantaneous data presented in Figs. 6 and 8 where the *Nu* number extremum track the supply pulsation frequency (e.g. there is one peak per mechanical pulsation frequency).

Fig. 9 shows an indicative cycle-averaged case with *Re* of 2366, H/R_b of 1.161, b_{min}/R_b of 0.131, θ of 20°, f_{mch} of 10 Hz, and with varying f_s/f_{mch} 1:1, 2:1, 3:1, 4:1 while Fig. 10 shows a case at a *Re* of 1683, H/R_b of 0.8, b_{min}/R_b of 0.05, and the same supply to mechanical frequency ratios. The data in both figures illustrate that the averaged CPRJR heat transfer displayed a wide range of *Nu* number magnitude, but have a similar profile with respect to the PRJR *Nu* data, labeled Mech Pulse in the figures. Note that averaged *Nu* values are presented in the legend.

A summary of the percent difference in average *Nu* number with respect to the purely mechanical (PRJR) *Nu* number is given in Table 1. The *Nu* data is arranged such that *Re*, non-dimensional height and gap width, mechanical forcing frequency and exit angle are read vertically down in a column. The corresponding supply to mechanical pulsing ratio and phase angle are arranged in rows. The PRJR (reference) *Nu* value for a given set of parameters is located vertically below the data for which it is a reference.

The range of *Nu* number for a given mechanical to supply pulsation ratio was approximately the same for all parameters tested. The average *Nu* numbers tended to increase as the mechanical pulsation frequency increased, and for a given mechanical pulsation, average *Nu* numbers typically increased as the supply frequency increased. The amount of entrained flow is proportional to the mean jet exit velocity and pulsation frequency, therefore as more flow is entrained from the ambient the *Nu* number increased.

CPRJR heat transfer within the toroidal vortex located between the nozzle centerline and the reattachment radius was typically greater than the corresponding PRJR case as seen in Fig. 9, where the heat transfer improved up to approximately 25% over the PRJR case in that region. And for the cases of lower non-dimensional flow guide height, heat transfer in this region was significantly improved with values up to 50% and was due to the greater influence of pulsation at a lower flow guide height. In general heat transfer improvements in the toroidal region were due to the flow rate at the flow-on supply pulsation position and decrease nozzle height with no evidence of boundary layer scouring via blowout.

The variation in non-dimensional flow guide height, H/R_b, and non-dimensional gap height, b_{min}/R_b, was coupled and limited numbers of cases were run in which the two parameters were varied. When the non-dimensional flow guide height was increased from 0.8 to 1.16 in conjunction with an increase of non-dimensional gap height from 0.05 to 0.13, a general reduction in all averaged *Nu* number from about 10% to 20% was observed; recall that the mechanical pulsation did not significantly affect heat transfer. The reattachment region for the 2:1 and 3:1 ratio cases for the higher non-dimensional flow guide height tended to straddle the mechanical case value. The trend was that the influence of any pulsation was lessened as the flow guide height was increased as momentum was lost due to flow interaction with the ambient because of the increase in mean path distance from the nozzle exit to the impingement surface.

The variation in the exit angle, θ, consisted of using the exit angle values of 0° and 20° in different test cases throughout this study. The effect of exit angle variation on the averaged *Nu* number was that the location of maximum *Nu* value was reduced by about 11% when the exit angle was varied from 0° to 20°; the PRJR *Nu* number also followed this trend. The average PRJR *Nu* number values increased by about 10% for the exit angle increase while

Table 1
Percent difference in average Nusselt number with respect to the PRJR Nusselt value rounded to whole value $(\frac{CPRJR-PRJR}{PRJR})$

Ratio|ω	2366						1683		*Re*
	1.161, 0.131				0.8, 0.05				H/R_b, b_{min}/R_b
	10				5		10		f_{mch}
	0	20	0	20	0	20	0	20	θ
1:1|0	11%	16%	9%	12%	15%	1%	21%	41%	
1:1|180	4%	16%	25%	23%	32%	22%	29%	47%	
2:1|0	10%	21%	25%	13%	51%	18%	38%	30%	
2:1|180	11%	19%	13%	15%	32%	10%	31%	24%	
3:1|0	15%	28%	21%	35%	41%	14%	−3%	56%	
3:1|180	15%	32%	18%	31%	51%	14%	25%	53%	
4:1|0	22%	33%	18%	33%	54%	22%	23%	58%	
4:1|180	31%	34%	24%	32%	53%	33%	22%	52%	
PRJR (reference)	39.6	47.2	48.2	53.4	37.6	52.3	38.6	40.2	

a corresponding change in CPRJR *Nu* number variation ranged from an increase of 15–22%. The larger reattachment radius value for $\theta = 0°$ was due to the flow being ejected parallel to the plate so that its impingement point was further from the nozzle centerline than the $\theta = 20°$ case, which ejected fluids more towards the plate. The lower heat transfer, for the $\theta = 0°$ case occurred as the mean path distance from the nozzle to the plate was greater than the $\theta = 20°$ case and flow energy was lost to the ambient.

Finally increasing *Re*, while holding all other parameters constant, resulted in increased local and averaged *Nu* numbers for all pulsation ratios. Generally the increased *Re* number caused similar percent increases in heat transfer for the 0° and 20° exit angle cases.

Summarizing the parameter influence in the local and averaged Nusselt numbers for the range of variables studied, the following observations are made:

1. PRJR frequency, f_{mch}, as evaluated in this study at 5 Hz and 10 Hz, has little influence on heat transfer. Mechanical pulsation does move the location of the reattachment radius slightly.
2. The larger Reynolds number produced greater heat transfer and larger radial locations of maximum *Nu* value. The increased heat transfer is attributed to the exiting air having greater momentum directed towards the impingement surface, greater entrainment from the ambient, and reduced mean distance to the surface. The variation in heat transfer caused by changing the Reynolds number is similar to that in PRJR nozzles.
3. Increasing the values of nozzle height and nozzle gap produced reattachment radii larger than the values associated with lower nozzle gap and flow guide height. Nozzle height and nozzle gap variation produced results similar to variation in PRJR nozzles.
4. Changing the exit angle in CPRJR nozzles from 0° to 20° produced a slight decrease in the radial location of maximum *Nu* and an increase in heat transfer.
5. The phase angle, ω, did not significantly affect the average surface heat transfer.

4. Conclusions

The results of this study show that combined pulsation Nusselt number is characterized by frequency interference of mechanical and supply pulsation effects. The reattachment radius is subject to the sweeping motion induced by the mechanical pulsation while extremum values of Nusselt number develop from the varying velocity magnitude of the supply pulsation mechanism. PSD analyses of the Nusselt number indicate the supply pulsation frequency generally dominates the mechanical pulsation frequency.

Significant improvement over the corresponding PRJR (mechanical pulsation) case was found to occur. The largest improvement in heat transfer occurred at the lower nozzle height with the exit angle of 20°. These improvements result from increased surface-directed momentum of the jet exit air flow and corresponding entrainment. For the range of parameters tested, combined pulsation did not appear to refresh the air within the toroidal vortex region under the nozzle or induce any thermal or velocity boundary layer instability that would lead to blowout.

References

Agnew, N.D., Elvery, K., Bremhorst, D.G., 1992. Modelling of a steady and fully pulsed reattaching radial jet. In: Australasian Fluid Mechanics Conference, vol. 2, pp. 1097–1100.

Beckwith, T., Marangoni, R.D., Lienhard, J., 1993. Mechanical measurements, fifth ed. Addison-Wesley Publishing Company, Reading Massachusetts.

Bremhorst, K., Agnew, N.D., 1999. Surface heat transfer of steady and fully pulsed radial reattaching nozzles. International Journal of Heat and Fluid Flow 20, 280–289.

Castleberry, J. 1997. Heat transfer characteristics of a pulsed radial reattachment nozzle. Master's thesis, Texas Tech University.

Furlow, J.S., 1999. Local instantaneous heat transfer characteristics from mechanical and supply pulsed radial reattaching nozzles, Master's thesis, Texas Tech University.

Furlow, J.S., James, D L., 1999. Local instantaneous convective heat transfer characteristics of radial reattaching nozzles. In: *National Heat Transfer Conference*, pp. NHTC99–151.

James, D., Castleberry, J., Pak, J.Y., 1999. Pulsed radial jet reattachment nozzle. International Journal of Heat and Mass Transfer 42, 2921–2933.

Laschefski, H., Holl, A., Grosse-Gorgemann, A., Mitra, N.K., Page, R.H., 1992. Flow structure and heat transfer of radial and axial jet reattachment on a flat plate. Fundamentals of Forced Convection Heat Transfer 210, 123–131.

Laschefski, H., Cziesla, T., Mitra, N.K., 1995. Influence of exit angle on radial jet reattachment and heat transfer. Journal of Thermophysics and Heat Transfer 9 (1), 169–174.

Nevins, R., Ball, H., 1961. Heat transfer between a flat plate and a pulsating impinging jet. In: Proceedings of the National Heat Transfer Conference, Boulder, CO, vol. 60, pp. 510–516.

Ostowari, C., Page, R.H., MacGregor, J.D., 1987. Heat transfer in a reattaching radial jet flow. In: Proceedings of the 1987 ASME-JSME Engineering Joint Conference, vol. 1, pp. 455–459.

Page, R.H., 1993. Axisymmetric gas jets: surface impingement phenomena. In: 14th Canadian Congress of Applied Mechanics, vol. 1, pp. 10–19.

Page, R., Hadden, L., Ostowari, C., 1989. Theory for radial jet reattachment flow. AIAA Journal 27 (11), 1500–1505.

Pak, J.Y., James, D., Parameswaren, S., 1999. Jet impingement characteristics from a pulsed radial jet reattachment nozzle. CFD Journal 7 (4), 451–462.

Seyed-Yagoobi, J., Narayanan, V., Page, R., 1998. Comparison of heat transfer characteristics of radial jet reattachment nozzle to in-line impinging jet nozzle. Journal of Heat Transfer 120, 335–341.

Sheriff, H., Zumbrunnen, D., 1994. Effect of flow pulsations on the cooling effectivness of an impinging jet. ASME Journal of Heat Transfer 116, 886–895.

Zumbrunnen, D., Aziz, M., 1993. Convective heat transfer enhancements due to intermittency in an impinging jet. ASME Journal of Heat Transfer 115, 91–98.